

EGL++: Extending Expected Gradient Length to Active Learning for Human Pose Estimation

Megh Shukla

Mercedes-Benz Research and Development India

megh.shukla@daimler.com

Abstract

State of the art human pose estimation models continue to rely on large quantities of labelled data for robust performance. Since labelling budget is often constrained, active learning algorithms are important in retaining the overall performance of the model at a lower cost. Although active learning has been well studied in literature, few techniques are reported for human pose estimation. In this paper, we theoretically derive expected gradient length for regression, and propose EGL++, a novel heuristic algorithm that extends expected gradient length to tasks where discrete labels are not available. We achieve this by computing low dimensional representations of the original images which are then used to form a neighborhood graph. We use this graph to: 1) Obtain a set of neighbors for a given sample, with each neighbor iteratively assumed to represent the ground truth for gradient calculation 2) Quantify the probability of each sample being a neighbor in the above set, facilitating the expected gradient step. Such an approach allows us to provide an approximate solution to the otherwise intractable task of integrating over the continuous output domain. To validate EGL++, we use the same datasets (Leeds Sports Pose, MPII) and experimental design as suggested by previous literature, achieving competitive results in comparison to these methods.

1. Introduction

The success of human pose estimation models [34, 23, 33, 4] in delivering robust performance has lead to its widespread adoption in various industrial applications such as driver monitoring systems. These applications often involve a large scale collection of annotated data to ensure optimal performance under various unbounded conditions. However, the capacity of these models come at the cost of an insatiable appetite for data. Often, costs associated with labelling large volumes of data are prohibitively expensive, necessitating the need for data efficient solutions.

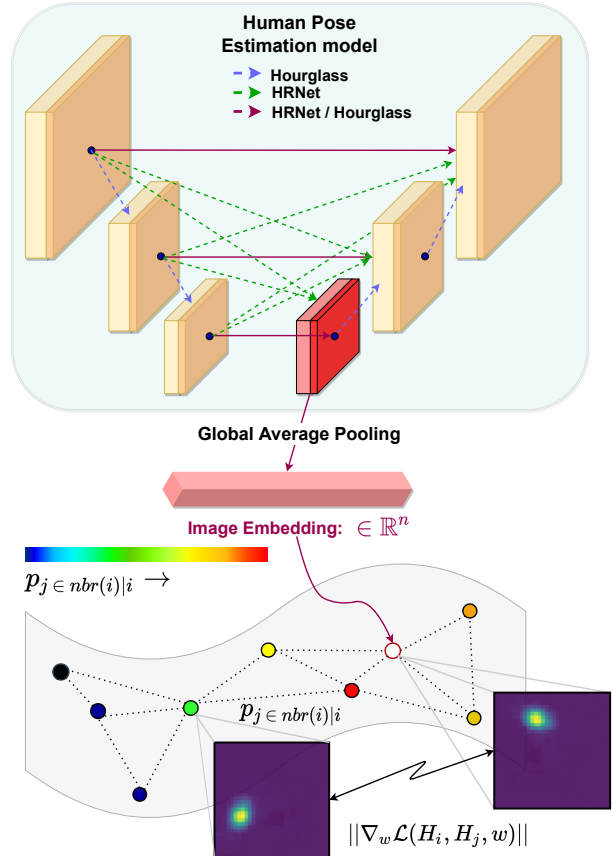


Figure 1. EGL++ generalizes expected gradient length to tasks where discrete probabilistic outputs are not available. In the absence of these probabilities, our expectation over the inferences for a given image uses a neighborhood probability distribution. The notion of neighbors for an (image, inference) pair uses low-dimensional representations from the pose model, allowing us to interpret inter-embedding distance into neighborhoods for each sample [36]. This neighborhood distribution quantifies the probability of various inferences being the target inference for the given sample. EGL++ uses this distribution over the inferences combined with the gradient induced by each inference to compute the expected gradient length for human pose estimation.

To reduce annotation costs, active learning algorithms select a small subset of unlabelled images for annotation in an effort to maintain model performance with fewer labelled images. This subset is obtained using the model’s feedback which ensures that the selected images impart new information for the model to learn. Active learning is a cyclical process with multiple iterations of selection-annotation-training until the model has achieved a desired level of performance, allowing for fast prototyping, lower data requirements (budget) and potentially limiting the bias in the training datasets.

Active learning algorithms differ in their methodology of sampling. These methods can roughly be grouped into categories such as diversity, uncertainty or ensemble based approaches. While diversity based approaches seek to introduce semantic variations in the labelled data, uncertainty based approaches quantify model ambiguity to select images for annotation. Ensemble approaches personify wisdom of the masses, with multiple models (actual/simulated) used to determine the annotation set. While active learning is well studied in literature with applications in classification and segmentation, relatively fewer techniques are transferable to human pose estimation. The challenge arises due to a multitude of factors, such as the lack of discrete labels as outputs, the absence of fully connected layers in state of the art pose estimation models or the need for regressing multiple joint heatmaps. This paper explores the application of expected gradient length [28], a classical active learning technique, in human pose estimation. Our two major contributions are:

1. We theoretically derive the formulation for expected gradient length - regression
2. We propose EGL++, a heuristic algorithm that allows us to extend active learning to human pose estimation

While expected gradient length for regression has been addressed in previous literature [5], this formulation is majorly intuition driven. We use statistical results that allow us to derive the formulation, and go one step ahead to prove that a closed form solution exists for linear regression. We then discuss practical considerations while implementing expected gradient length, leading us to a new heuristic algorithm: EGL++. With EGL++, we propose a model agnostic algorithm that generalizes expected gradient length to tasks where discrete probabilistic outputs are not available. We show that an alternative interpretation of the formulation leads us to computing internal representation of the images to obtain conditional probabilities associated with expected gradient length. We also take into account practical considerations while implementing EGL++ [10]. We compare EGL++ with other state of the art active learning for human pose estimation algorithms, achieving statistically significant result at the 90% confidence level.

2. Related Work

Active Learning: Any discussion on active learning would be incomplete without mentioning Settles’ survey [28] detailing various classical methods and their applications. Algorithms that employ uncertainty have a rich history, with early works including [18, 14]. These algorithms typically include variations of entropy and maximum margin that utilize the softmax outputs of the model. Recent works include [21] which uses generative adversarial networks to generate high entropy samples for multi-class problems, and [15] which employs uncertainty techniques for region based segmentation.

Ensemble based approaches [3, 17, 22] build upon the Query by Committee paradigm, using multiple models to make the active learning annotation set selection. [22] uses artificial training data to construct diverse committee members, whereas [3] uses ensemble learning and presents its comparison with recent active learning techniques on classification datasets. [17] uses cues from the softmax outputs in classification to show the usefulness of maximum margin in a multi-class setting.

Diversity based approaches [37, 7, 27] as the name suggests seek to incorporate a high degree of variation in the sampled set of unlabelled images. Core-set [27] remains a popular approach that utilizes the linearly separable embedding space produced by the penultimate fully connected layer in classification networks. Core-set remains one of the few techniques transferable to a wide range of tasks including human pose estimation, even though the linearly separable embedding space requirements are not met.

Bayesian approaches have found novel applications in active learning, with [9, 16] providing theoretical results to estimate uncertainty in the network output. These approaches rely on estimating the aleatoric and epistemic uncertainties with bayesian neural networks to quantify the ambiguity associated with data and network inferences. Derivatives of this work include [6] which use bayesian uncertainty approaches for hand pose estimation.

Our literature survey points us to various exciting active learning paradigms, however, few techniques can be readily applied to human pose estimation. Uncertainty based approaches rely on softmax activations, limiting their use in human pose estimation where the heatmaps are regressed. Ensemble models rely on majority through voting, which again is heavily biased towards classification. Core-Set, a diversity based algorithm finds applications in a wide range of tasks due to the versatility associated with it. Following [38], we include Core-Set in our comparison studies. While Bayesian Active Learning has provided beautiful theoretical results for classification and segmentation, the authors to the best of their knowledge are not aware of similar implementations in human pose estimation. Some close works include bayesian hand pose estimation [6], however the net-

work architecture and inputs differ significantly from human pose estimation. Aleatoric uncertainty has been effectively used in body joint occlusions [11], however the algorithm does not cater to active learning. Concerns [27, 38] also remain on scalability of bayesian methods to large datasets.

Expected Gradient Length: Expected gradient length [28] utilizes the gradient norm in determining the most informative samples. Early works [30, 29, 39] successfully leveraged expected gradient length in classification and text. Huang *et al.* [12] show that expected gradient length is a consequence of reducing the variance of the estimator over the testing set. Zhang *et al.* [40] use expected gradient length for sentence and document classification using CNNs. While previous methods worked with discrete outputs, [5] demonstrates the use of expected gradient length in regression. To circumvent the lack of discrete outputs, the method uses an ensemble as a monte carlo approximation of the expectation. We discuss this paper thoroughly in the methodology section.

Active learning - Human Pose Estimation: Liu and Ferrari [19] introduced active learning for human pose estimation, proposing multi-peak entropy as an uncertainty cue, while also using an auxiliary model that provides distance cues. Learning Loss [38] uses an auxiliary model that takes as input intermediate features from the model to predict the ambiguity associated with the image. LearningLoss++ [2] provides a mathematically driven background for Learning Loss, with a heavy emphasis on the ability of the module to detect failures. This paper in contrast emphasizes on a different active learning paradigm, with a focus on improving the process of active learning in general. EGL++ focuses on the degree of change in the pose estimation model instead of uncertainty cues. Since embeddings in the feature space exhibit semantic continuity, with similar features often grouped together, this observation allows us to formulate active learning as an expected gradient length problem by measuring the disagreement in the inferences produced between neighbours.

Revisiting Expected Gradient Length: The formulation for expected gradient length as defined in [28, 29] is shown in Eq: 1, where $l(\cdot)$ represents the loss function and $\{x, y\}$ represent the input and the softmax vector output.

$$x^* = \arg \max_x \sum_i P(y_i|x; \theta) \|\nabla_{\theta} l(\mathcal{L} \cup \{x, y_i\}; \theta)\| \quad (1)$$

Eq: 1 shows the approximation of the expected gradient for classification tasks. The conditional probability term represents the softmax output for a given class y_i , with the gradient computed assuming y_i is the correct label for the input x . However, as noted in the original paper, this approach is computationally expensive, and is also not representative of tasks where discrete probabilistic outputs are not available.

To overcome the lack of labels, Cai *et al.* extended expected gradient length to regression by building an ensemble of models. Let $\mathcal{F}^K = \{f_1, f_2 \dots f_K\}$ represent a set of hypothesis obtained by training on subsets of labelled data $z = \{(x_1, y_1), (x_2, y_2) \dots (x_N, y_n)\}$ and f_z obtained by training on the entire pool of labelled data. Then, the sampling formulation can be represented as:

$$x^* = \arg \max_x \frac{1}{K} \sum_{k=1}^K \|(f_z(x) - f_k(x))x\| \quad (2)$$

Eq: 2 uses a committee of hypothesis to approximate the change induced by the sample x in the original model f_z . Therefore, the samples picked for annotation are those where there is higher level of disagreement between the model f_z and various weak learners f_k .

3. EGL++

We first present a theory on expected gradient length for regression, followed by a detailed discussion on EGL++. We also discuss some practical considerations to account for when implementing the algorithm.

3.1. Theory

We mathematically support the intuition behind Eq: 2, using a variation of the established proof [12]. We briefly discuss the No Free Lunch theorem to support our derivation. We later discuss the challenges associated with such an ensemble formulation, paving the way for EGL++.

The No Free Lunch Theorem: Shalev-Shwartz and Ben-David accurately summarize the essence of the No Free Lunch theorem in a single sentence: *there is no such universal learner; no learner can succeed on all learning tasks.* This arises due to the uncertainty associated with the unseen samples. For any function that fits on any training dataset, adversarial samples can be drawn causing the function to perform poorly on those samples. This is formalized in Theorem 5.1 [31], we urge the interested reader to follow it for a formal proof.

A direct interpretation of the theorem is that for observed samples z_{obs} , *multiple hypothesis including θ_0 , the true hypothesis, can explain z_{obs} , due to the ambiguity associated with the unknown distribution.* This allows us to model the family of hypothesis as a probability distribution $q(\theta|z_{obs})$ over the parameter space and conditioned on the observed variables. Naturally, as we draw more samples from the unknown distribution $p(x, y)$, the parameter space that can explain the observed samples is restricted further.

3.1.1 Ensemble Approach - Linear Regression

As a consequence of the no free lunch theorem, we propose a variation of the proof presented in [32, 12, 20], allowing

us to derive Eq. 2. Let $\mathcal{Z} \in \{\mathcal{X} \times \mathcal{Y}\}$ represent the domain over which we train a model θ and z_{obs} represent the observed samples. Following Huang *et al.*, we model the joint distribution as: $p(x, y|\theta_0) = p(y|x, \theta_0)p(x)$. Here, θ_0 parameterizes the true distribution p over \mathcal{Z} which we wish to learn. At this stage, the original proof defines a new distribution q for the observed values z_{obs} , which is defined as $q(x, y|\theta_0) = p(y|x, \theta_0)q(x)$ where $q(x)$ reflects the observed samples x in z_{obs} . However, this definition contains an implicit assumption that θ_0 alone describes z_{obs} which is not true. Our previous discussion on the no free lunch theorem allows us to model z_{obs} as the expectation over the parameter space due to the existence of multiple plausible hypothesis for z_{obs} :

$$\begin{aligned} q(x, y) &= \mathbb{E}_\theta [q(y|x, \theta)q(x)] \\ &= \int_\theta q(y|x, \theta)q(x)\pi(\theta|z_{obs})d\theta \end{aligned} \quad (3)$$

One can argue that Eq. 3 is a consequence of conditional probability and marginalization, however the no free lunch theorem allows for the existence of multiple plausible hypothesis for the observed samples, making this variation significant. The proof proceeds further using a well known result on the asymptotic convergence of model parameters to its true value involving Fisher Information: $\sqrt{n}(\hat{\theta} - \theta^*) \xrightarrow{D} \mathcal{N}(0, I_q^{-1}(\theta^*))$. Using this result, Huang *et al.* argue that one way of converging to the true parameters (LHS) is by maximizing the Fisher Information with respect to the training distribution q . (minimizing the inverse). This is equivalent to maximizing $\mathbb{E}_{q(x, y)} [\nabla_\theta l(x, y, \hat{\theta}) \nabla_\theta^T l(x, y, \hat{\theta})]$. Using Eq. 3, we show that this is equivalent to maximizing:

$$q^* = \arg \max_q \int_x q(x) \int_y \int_\theta q(y|x, \theta) \pi(\theta|z_{obs}) \|\nabla_{\theta_0} l(x, y, \theta_0)\|^2 d\theta dy dx \quad (4)$$

Since integrating over the parameter space is intractable, we approximate $\pi(\theta|z_{obs})$ by bootstrapping and building an ensemble of weak learners (linear models) $q(\theta_i|z_i)$, where $z_i \subset z_{obs}$ using maximum likelihood. Also, statistical linear regression results [24] show that $q(y|x, \theta_i)$ is gaussian distribution with a closed form mean and prediction variance $\mathcal{N}(\mu(\theta_i, x), \sigma(z_{obs}))$. Next, we define f_z to be the function trained on all z_{obs} , with θ_z our best estimate of the true parameters θ_0 . Finally, we note that finding a training distribution q that maximizes the expected gradient is same as including the sample x having the highest expected gradient in the training set [12]. Using the Fubini-Tonelli

theorem to reorder summation-integration, we get:

$$x^* = \arg \max_{x \in \text{unlabelled}} \left[\frac{1}{K} \sum_{k=1}^K \int_{-\infty}^{\infty} \frac{1}{\sqrt{2\pi}\sigma_k(z_{obs}^{(k)})} \frac{(y - \mu_k(x))^2}{2\sigma_k^2(z_{obs}^{(k)})} [(f_z(x) - y)x]^2 dy \right] \quad (5)$$

Note that we have substituted $l(x, y, \theta_0)$ in Eq. 4 with the regression mean square error for the model f_z . On comparing with Cai *et al.* (Eq. 2), we note that the gradient term in our formulation is squared as a result of maximizing the Fisher Information. Also Eq. 2 is equivalent to Eq. 5, if exactly one sample y_i is drawn from $q(y|x, \theta_i)$ for each $i \in K$ corresponding to the mode of the distribution.

Eq. 5 has a closed form solution. Let $(y - f_z(x))^2 = [(y - \mu_k) + (\mu_k - f_z)]^2$. The integral can be reduced to: $\int \mathcal{N}(y, \mu_k, \sigma_k)(y - \mu_k)^2 dy + 2 \int \mathcal{N}(y, \mu_k, \sigma_k)(y - \mu_k)(\mu_k - f_z) dy + \int \mathcal{N}(y, \mu_k, \sigma_k)(\mu_k - f_z)^2 dy$. The first term corresponds to the variance of the normal distribution, the second term results in a zero as the means cancel out and the last term coefficient is independent of y , resulting in $(\mu_k - f_z)^2$. We request the reader to refer to the supplementary material for a complete derivation. The final closed form solution for Eq. 5, completing our derivation is:

$$x^* = \arg \max_{x \in \mathcal{U}} \left[\frac{\|x\|^2}{K} \sum_{k=1}^K (\sigma_k^2 + (\mu_k(x) - f_z(x))^2) \right] \quad (6)$$

3.2. Algorithm

Eq. 4 represents generalized expected gradient length tasks, which we have further analyzed for linear regression (Eq. 6). We note that estimating the conditional probability for complex tasks [8] using multiple forward propagation is computationally expensive, raising concerns regarding scalability to large datasets. We also have access to only a small labelled pool of images during the initial stages of active learning, limiting the use of bootstrap techniques. We therefore reduce Eq. 4 to address active learning for human pose estimation with a single model ($K=1$), relying on a single forward pass. We define the problem as:

$$x^* = \arg \max_{x \in \text{unlabelled}} \sum_{n=1}^{n=N} q(y_n|x, \theta) \|\nabla_\theta l(x, y_n, \theta)\|^2 \quad (7)$$

The main task is to estimate $q(y|x, \theta)$ for any arbitrary model and input. A heuristic based approach takes us into the field of dimensionality reduction, which explicitly allow us to model the conditional probability between various representations. Before we discuss the usefulness of two such algorithms: t-SNE [36] and Locally Linear Embedding [26], we need to first construct internal representations of images x that would act as inputs to these algorithms.

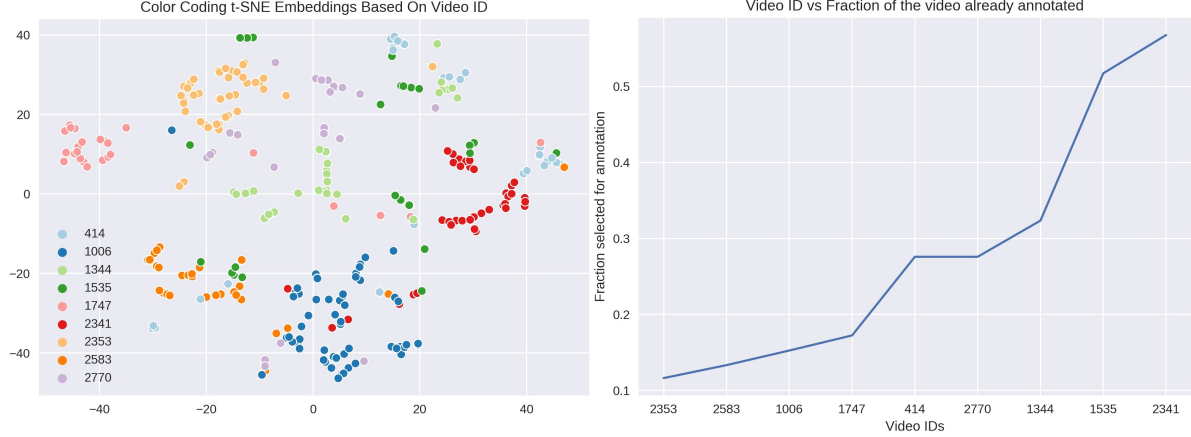


Figure 2. (Left) t-SNE visualization of the embeddings color-coded by video. (Right) Fraction of frames per video previously chosen by EGL++ for annotation. We first note that temporally related frames from the same video have similar embeddings. Videos (2353, 2583, 1006) that have embeddings concentrated in a small volume are lightly sampled, whereas videos (2341, 1535, 1344) where the embeddings are dispersed tend to be more heavily sampled by EGL++. Dispersion indicates a *weakly sampled* neighborhood in which each sample has a high expected gradient, making them likely candidates to be annotated.

Low Dimensional Representation

Introducing low dimensional representations has two major benefits. Not only does a smaller representation improve the compute time taken for subsequent algorithms, low dimensional representations allow for the model’s feedback which would otherwise have been absent if we considered an input image in its entirety. These representations present us with a perspective on how the model views input images, and more importantly, how the model finds semantic meaning across the pool of images. Multiple popular human pose estimation models and their variants employ a top-down approach that involves capturing features at various scales (Fig: 1). The top-down approach therefore acts similar to an autoencoder, with a compressed form of the original image at the lower layers in the top-down approach. Not only do these embeddings capture high-level features from the network, extracting them from the coarsest resolution allows us to get a global view of the image. Since these representation are three dimensional tensors, we collapse the spatial dimensions using global average pooling to obtain a vector embedding (h) of the input image. Subsequently we define an *image-embedding-heatmap* triplet, with an emphasis on the $\{\text{embedding} - \text{heatmap}\}$ pair. Next, we show that this $(h - y)$ pair allows us to develop a heuristic that approximates the true conditional distribution in Eq: 7.

Conditional Probability

Dimensionality reduction algorithms seek to reproduce the spatial representation between high dimensional samples in lower dimensions. These algorithms differ in the way they model this high dimensional space. In particular, t-SNE and Locally Linear Embedding solve for the weights of a neighborhood graph imposed on the embeddings.

In both the algorithms, the weights can be interpreted as conditional probabilities. Locally Linear Embedding (LLE) solves for the weight matrix: $W^* = \arg \min_W \sum_i |X_i - \sum_j w_{ij} X_j|^2$ subject to the constraint $\sum_j w_{ij} = 1$. As the objective suggests, each vector w_i tries to reconstruct X_i from its neighbours X_j . If we impose an additional constraint $w_{ij} \geq 0$ alongside $\sum_j w_{ij} = 1$, we can interpret w_{ij} as the probability of X_j being a neighbour of X_i . Although technically beautiful, the approach has a high time complexity (nearest neighbors: $O(dN^2)$ weights: $O(dNK^3)$) where d is the number of features, N represents the number of samples, and K represents the number of neighbors used for reconstruction. In comparison, computing the neighborhood probability matrix in t-SNE has a time complexity of $O(dN^2)$, with a high degree of GPU parallelism available. t-SNE is also well studied with a wide spread adoption of the algorithm as the *de-facto* dimensionality reduction tool.

t-SNE: t-SNE [36, 35] proposes a two stage process: defining a neighborhood probability distribution on the original samples and replicating the same in low dimensional spaces. We use the Stochastic Neighborhood Embedding based conditional distribution to describe the relation between our embeddings (h) from the previous stage:

$$q(h_j|h_i, \theta) = \frac{\exp(-\|h_i - h_j\|^2/2\sigma_i^2)}{\sum_{k \neq i} \exp(-\|h_i - h_k\|^2/2\sigma_i^2)} \quad (8)$$

Intuitively, Eq: 8 corresponds to the probability of h_j being in the neighborhood of h_i . For every sample i , a gaussian distribution is defined with a variable σ_i unique to each sample. This σ_i allows for variable density among the embeddings, allowing a soft degree of control on the spatial

extent of the neighborhood of h_i .

Since we know the fixed set of ground truth heatmaps y_j for each embedding h_j when image x_j is from the labelled set, our heuristic lies in approximating $q(h_j|h_i, \theta)$ with $\hat{q}(y_j|h_i, \theta)$, the probability of y_j being the true heatmap for x_i . We divide our embeddings into labelled $h_{\mathcal{L}}$ and unlabelled sets $h_{\mathcal{U}}$ where we identify the neighborhood for each $h \in \mathcal{U}$ in terms of all $h \in \mathcal{L}$. This results in a conditional probability matrix $q(h_{\mathcal{L}}|h_{\mathcal{U}}, \theta) = \hat{q}(y_{\mathcal{L}}|h_{\mathcal{U}}, \theta)$ of shape $(|\mathcal{U}| \times |\mathcal{L}|)$, allowing us to compute the expectation for $\|\nabla_{\theta} l(x_{\mathcal{U}}, y_{\mathcal{L}}, \theta)\|^2$.

Gradient Computation

In an idealistic world, where silicon clock speeds are measured in terahertz and deep learning models train instantaneously, gradient computations would nary have been an issue. Alas, that is not the case, and EGL++ needs fast yet efficient heuristics for gradient computation. Previously, we have computed a conditional probability matrix where each element a_{ij} represents $\hat{q}(y_j|h_i, \theta)$. This is used in calculating the expected gradient length $\sum_j \hat{q}(y_j|h_i, \theta) \|\nabla_{\theta} l(\theta(x_i) - y_j)^2\|^2$ for the unlabelled sample x_i . Computing this value for all instances of y_j an expensive task, especially when most values of $\hat{q}(y_j|h_i, \theta) \approx 0$. Instead, we restrict y_j to be among the top-K most probable values given by $\hat{q}(y_j|h_i, \theta)$, limiting the number of gradient computations needed.

To further reduce computational costs, we use Goodfellow’s technique for efficient per example gradient computation [10]. Popular deep learning frameworks aggregate the gradients across the minibatch during the optimization process, losing out on individual gradients. While computing individual gradients with a batch size of one is possible, such an approach is excruciatingly slow. Goodfellow’s solution uses intermediate activations and hidden representations to compute the gradient using convolutional and linear layers for each sample x_j in the mini-batch. While this is not the true gradient for x , (for *e.g.*, no batch normalization gradients) this heuristic allows for fast computations of gradients in a single forward pass.

We also briefly discuss the parallelization potential with the gradient computation. Recall that our task is to compute the gradients for each unlabelled sample x_i for the top-k mostly likely inferences. Since the gradient for each x_i is independent of others, multiprocessing can be used to parallelize the process of gradient computation across the unlabelled set \bar{x}_i . Gradient computation for individual x_i can be performed in parallel on the GPU, with a process similar to that of training a model. Normally, the process of computing gradients during training involves sampling a mini-batch \bar{x} of different inputs, performing model inference, calculating the loss with respect to the ground truth \bar{y} and computing the gradient. Instead of sampling different

inputs for the mini-batch, we construct a mini-batch with clones of x_i that allows us to capture gradients with respect to different y_j for the same x_i .

Once we have obtained the pairwise gradients between \bar{y}_j and \bar{x}_i , computing the expected gradient length is reduced to a hadamard product between the conditional probability matrix $\hat{q}(y_j|x_i, \theta)$ and the gradient norm matrix $\|\nabla_{\theta} l(\theta(x_i) - y_j)^2\|^2$ followed by a summation along j . Samples with the highest expected gradient lengths are selected for annotation.

Algorithm 1: EGL++

Input: Human pose estimator (f), Number of neighbors (\mathcal{K}), Budget (\mathcal{B})

Output: Unlabelled images ($x_{\mathcal{U}}^*$) for annotation

Data: Labelled ($x_{\mathcal{L}} - y_{\mathcal{L}}$) and Unlabelled ($x_{\mathcal{U}}$) images

```

1  $h_{\mathcal{U}} = f_{enc}(x_{\mathcal{U}})$  // encodings for labelled
2  $h_{\mathcal{L}} = f_{enc}(x_{\mathcal{L}})$  // encodings for unlabelled
3 Compute matrix  $q(h_j|h_i, \theta)$  using Eq: 8, where
    $i \in \mathcal{U}$  and  $j \in \mathcal{L}$  // Size  $(|\mathcal{U}| \times |\mathcal{L}|)$ 
4  $\hat{q}(y_j|h_i, \theta) = q(h_j|h_i, \theta)$  // Heuristic,  $h_j \rightarrow y_j$ 
5 Initialize  $\{\theta_{fast} : \theta_0 \text{ layers} \in \text{linear, conv}\}$ 
6  $(\hat{q}(y_j|h_i, \theta), y_j) = \text{top} - \mathcal{K}(\hat{q}(y_j|h_i, \theta), y_j)$ 
   /* CPU multiprocessing - parallelize for */
   /* Final gradient matrix size:  $|\mathcal{U}| \times |\mathcal{K}|$  */
7 for  $x_i$  in  $\mathcal{U}$  do
   /* Fast Gradient Approximation */
   /* GPU parallel across  $j$  for each  $i$  */
8   Compute gradient norm  $\|\nabla_{\theta_{fast}} f(x_i), y_j\|^2$ 
   /* Expectation is hadamard product  $\hat{q} \circ \nabla$ ,
      reduce summed along  $j$ . Shape:  $|\mathcal{U}|$  */
9    $\bar{\mathbb{E}}_y[\nabla_{\theta}(y, x_{\mathcal{U}}, \theta)] =$ 
      $\sum_j \hat{q}(y_j|h_i, \theta) \circ \|\nabla_{\theta_{fast}} f(x_i), y_j\|^2$ 
10 return  $x_{\mathcal{U}}^*$ : Return samples corresponding to top -  $\mathcal{B}$ 
    expected gradients from  $\bar{\mathbb{E}}_y[\nabla_{\theta}(y, x_{\mathcal{U}}, \theta)]$ 
```

EGL++: More Than The Sum Of Its Parts

The interplay between the three components (representation-probability-gradients) allows EGL++ to comfortably outperform state of the art in active learning for human pose estimation. While closed form solutions (Eq: 6) are not available for all but the simplest cases, with EGL++ we frame a heuristic algorithm (1) to approximate Eq: 4 without the need for multiple inferences / ensemble models. While low dimensional representations capture the essence of an image, the neighborhood graph quantifies the degree of relation between these representations, with the gradients finally measuring the dissimilarity between these related representations. The end outcome is that of synergy between the components!

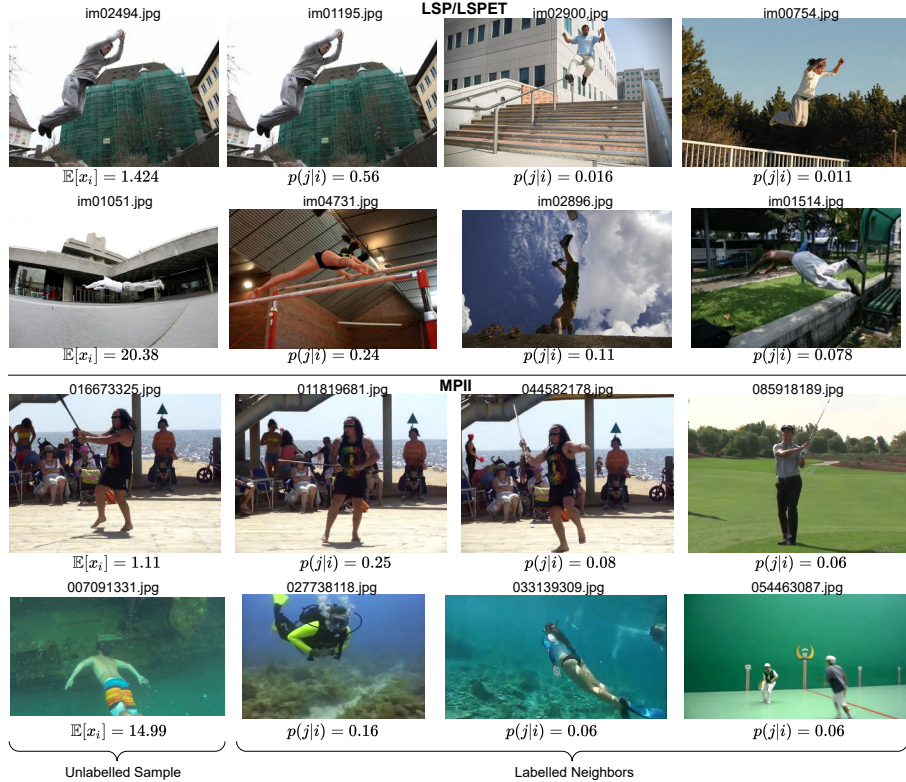


Figure 3. Quantifying the expected gradient length for unlabelled images (first column) along with the labelled images corresponding to the highest neighborhood probabilities. We show both: the image having highest as well as lowest expected gradient length for LSP-LSPET and MPII. We observe that for images with the smallest length, we already have annotated images similar to the labelled image. Whereas the unlabelled images having the highest gradient length correspond to difficult poses with weak model outputs as well as contain a hint of overfitting (bottom row: emphasis on background?).

4. Experiments and Results

Experimental Design: The PyTorch [25] code for our experiments is available on [GitHub Anonymized]. We compare our algorithm with three state of the art algorithms: Coreset [27], Multi-peak entropy [19] and Learning Loss [38]. We simulate multiple cycles of active learning, with each cycle selecting 1000 new images for annotation. A base model trained on an initial 1000 images is shared by all algorithms. To ensure consistency, we conduct 5 independent runs for each cycle, and report the mean and standard deviation for these runs. Also, we conduct a paired t-test to measure the significance of our results at a 90% confidence level. Following multi-peak entropy and learning loss, we use the MPII [1] and LSP [13] human pose datasets. The MPII dataset consists of images corresponding to everyday human activity, whereas LSP emphasizes on sporting activities. For MPII, we report our results on the Newell validation split [23] as done in (Liu and Ferrari) and (Yoo and Kweon) for the MPII dataset. We select 1000 images randomly from the training dataset to train our base models. We use the LSP authors’

data split, with the first 1000 images of the LSP dataset used to train the base models, and the last 1000 images acting as the testing set. The entire LSPET dataset is used as the unlabelled pool for active learning sampling. Wherever possible, we have used open source code for our experiments. We use the original Stacked Hourglass [23] with two stacked hourglasses as the human pose estimator, though noting that EGL++ is model agnostic. Following Multi-Peak Entropy, we extract single persons into separate images if the underlying image contains multiple persons. We also use standard evaluation metrics: PCKh@0.5 for MPII and PCK@0.2 for LSP-LSPET.

Results and Discussion

We first discuss the intuition behind the working of EGL++. Fig: 2 and Fig: 3 go hand in hand in describing the intuition, with the former providing a qualitative assessment and the latter a quantitative one. Fig: 2 plots the color-coded embeddings corresponding to videos having the highest representation in the MPII training dataset; also showing what fraction of a video has been sampled at the end of the fifth

MPII Newell Validation Split: Mean+-Sigma (5 runs), one-tailed paired t-test (vs EGL++) at 0.1 significance value															
#images →	2000			3000			4000			5000			6000		
Methods	μ	σ	p	μ	σ	p	μ	σ	p	μ	σ	p	μ	σ	p
Random	0.7595	0.055	0.003	0.7833	0.0065	0.012	0.8031	0.0091	0.006	0.8135	0.0041	0.001	0.8223	0.0074	0.007
Core-set [27]	0.7661	0.006	0.0047	0.7924	0.007	0.245	0.8125	0.0067	0.072	0.8223	0.0114	0.123	0.8297	0.0111	0.064
Multi-peak [19]	0.7674	0.0061	0.0054	0.7956	0.0046	0.462	0.8119	0.0031	0.063	0.8261	0.005	0.093	0.8311	0.0071	0.062
Learning Loss [38]	0.7628	0.0076	0.0276	0.7927	0.0052	0.185	0.8135	0.0035	0.152	0.8294	0.0044	0.319	0.8379	0.0046	0.053
EGL++ (ours)	0.7728	0.0063	-	0.7958	0.0033	-	0.8153	0.0051	-	0.8307	0.0025	-	0.84	0.0038	-

LSP Test Split: Mean+-Sigma (5 runs), one-tailed paired t-test (vs EGL++) at 0.1 significance value															
#images →	2000			3000			4000			5000			6000		
Methods	μ	σ	p	μ	σ	p	μ	σ	p	μ	σ	p	μ	σ	p
Random	0.8034	0.0031	0.285	0.8181	0.0024	0.297	0.8268	0.0032	0.138	0.8335	0.0036	0.095	0.8413	0.0016	0.029
Core-set [27]	0.7969	0.0082	0.043	0.8141	0.0045	0.096	0.8225	0.0039	0.021	0.8311	0.0038	0.032	0.8373	0.0031	0.006
Multi-peak [19]	0.8036	0.004	0.225	0.8148	0.0053	0.125	0.8263	0.0023	0.119	0.8329	0.002	0.036	0.843	0.0044	0.063
Learning Loss [38]	0.7958	0.0039	0.002	0.8139	0.0034	0.071	0.8231	0.0042	0.038	0.8331	0.0025	0.029	0.842	0.0053	0.098
EGL++ (ours)	0.8049	0.0045	-	0.8191	0.0027	-	0.8303	0.0043	-	0.8391	0.0051	-	0.8468	0.0036	-

Table 1. (Active Learning Simulation) We compare EGL++ with state of the art active learning algorithms for human pose estimation on the MPII and LSP-LSPET datasets. We train five base models on 1000 images, acting as the initial set of pretrained models for the first active learning cycle. Subsequent cycles use the pretrained model from the predecessor to sample a new set of 1000 images.

cycle. A quick glance highlights the semantic relation between embeddings, which allows us to build a neighborhood graph in the embedding space. This neighborhood graph allows us to quantify the dissimilarity (Fig: 3) between a sample and its neighbors using the expected gradient length formulation. Comparisons with Core-set naturally arise since both the techniques use embeddings in the core algorithm. Like Core-set, EGL++ too could be characterized as a diversity promoting technique, albeit in a different manner. While core-set uses the absolute euclidean distance as a notion of dissimilarity between two semantically different images, EGL++ uses the same metric to measure the degree to which two *similar* image-inference pairs differ, as seen in Fig: 3. Core-set has been used in classification to a great degree of success, since classification guarantees the linear separability of the penultimate layer embeddings, making euclidean distance relevant to measure the degree of dissimilarity. However, no such guarantees to estimate dissimilarity are available with regression, for an n -dimensional space the notion of distance may wildly differ across various dimensions. EGL++ harnesses t-SNE’s ability to model neighbors and their associated heatmaps accurately, while using gradient computations to quantify the dissimilarity of a sample with its neighbors.

Comparison on MPII/LSP-LSPET: We also simulate multiple active learning cycles and compare the results (Table: 1). We show that our algorithm achieves statistically significant result (90% confidence level) across many active learning cycles and when compared with multiple algorithms. MPII and LSP-LSPET allow us to examine the behavior of algorithms under two different conditions: when the labelled and unlabelled pool follow the same distribution of images (MPII), and when the pools differ (LSP - initial labelled, LSPET - unlabelled). While active learning algorithms are significantly different from random sampling for MPII, this generalization does not hold true for LSP-LSPET. However we note that even in this setting,

EGL++ achieves statistically significant results over other algorithms indicating the ability to generalize to unseen distributions. For the MPII dataset given enough cycles the learning loss method is successfully able to identify patterns to accurately select images which it considers *lossy*. We also observe that Core-Set does not extend well to human pose estimation, which we believe is due to linear separability of the penultimate layer embeddings not being enforced for human pose estimation. Multi-peak entropy fares well in the initial phases of active learning with its performance declining in the subsequent stages. Entropy for active learning has been well studied in [38], and while multi-peak entropy fares better than vanilla entropy, it shares the same weaknesses as its predecessor. Learning Loss and its variants are a special category of active learning algorithms with an emphasis on detecting faulty inferences. We believe that an active learning strategy for human pose estimation should involve both: iteratively sampling and annotating faulty inferences as well as generalized sampling (EGL++) to improve the general performance of the models.

5. Conclusion

In this paper, we study expected gradient length and develop a heuristic algorithm for active learning in human pose estimation. While the formulation for expected gradient length in linear regression is intuitively driven, our first contribution is in using established statistical results to derive and prove that a closed form solution for linear regression exists. We then discuss the limitations of this formulation for practical applications. Based on this derived result, our second contribution lies in proposing a heuristic based algorithm, EGL++, that removes the necessity of an ensemble or performing multiple inferences in computing the gradient length. We show that multiple heuristics when combined together form a formidable algorithm which delivers statistically significant results, outperforming its counterparts on the LSP and MPII datasets.

References

- [1] Mykhaylo Andriluka, Leonid Pishchulin, Peter Gehler, and Bernt Schiele. 2d human pose estimation: New benchmark and state of the art analysis. In *IEEE Conference on Computer Vision and Pattern Recognition (CVPR)*, June 2014. 7
- [2] Anonymous. Learningloss++: Revisiting active learning for human pose estimation, 2021. Concurrent Submission, `concurrent.pdf`. 3
- [3] William H Beluch, Tim Genewein, Andreas Nürnberger, and Jan M Köhler. The power of ensembles for active learning in image classification. In *Proceedings of the IEEE Conference on Computer Vision and Pattern Recognition*, pages 9368–9377, 2018. 2
- [4] Adrian Bulat, Jean Kossaifi, Georgios Tzimiropoulos, and Maja Pantic. Toward fast and accurate human pose estimation via soft-gated skip connections. In *2020 15th IEEE International Conference on Automatic Face and Gesture Recognition (FG 2020)(FG)*, pages 101–108. IEEE Computer Society. 1
- [5] W. Cai, Y. Zhang, and J. Zhou. Maximizing expected model change for active learning in regression. In *2013 IEEE 13th International Conference on Data Mining*, pages 51–60, 2013. 2, 3
- [6] Razvan Caramalau, Binod Bhattarai, and Tae-Kyun Kim. Active learning for bayesian 3d hand pose estimation. In *Proceedings of the IEEE/CVF Winter Conference on Applications of Computer Vision*, pages 3419–3428, 2020. 2
- [7] Ehsan Elhamifar, Guillermo Sapiro, Allen Yang, and S Shankar Sasrty. A convex optimization framework for active learning. In *Proceedings of the IEEE International Conference on Computer Vision*, pages 209–216, 2013. 2
- [8] Yarin Gal and Zoubin Ghahramani. Dropout as a bayesian approximation: Representing model uncertainty in deep learning. In *international conference on machine learning*, pages 1050–1059. PMLR, 2016. 4
- [9] Yarin Gal, Riashat Islam, and Zoubin Ghahramani. Deep bayesian active learning with image data. *arXiv preprint arXiv:1703.02910*, 2017. 2
- [10] Ian Goodfellow. Efficient per-example gradient computations, 2015. 2, 6
- [11] Nitesh B Gundavarapu, Divyansh Srivastava, Rahul Mitra, Abhishek Sharma, and Arjun Jain. Structured aleatoric uncertainty in human pose estimation. In *CVPR Workshops*, volume 2, 2019. 3
- [12] Jiaji Huang, Rewon Child, Vinay Rao, Hairong Liu, Sanjeev Satheesh, and Adam Coates. Active learning for speech recognition: the power of gradients, 2016. 3, 4
- [13] Sam Johnson and Mark Everingham. Learning effective human pose estimation from inaccurate annotation. In *Proceedings of IEEE Conference on Computer Vision and Pattern Recognition*, 2011. 7
- [14] Ajay J Joshi, Fatih Porikli, and Nikolaos Papanikolopoulos. Multi-class active learning for image classification. In *2009 IEEE Conference on Computer Vision and Pattern Recognition*, pages 2372–2379. IEEE, 2009. 2
- [15] Tejaswi Kasarla, Gattigorla Nagendar, Guruprasad M Hegde, Vineeth Balasubramanian, and CV Jawahar. Region-based active learning for efficient labeling in semantic segmentation. In *2019 IEEE Winter Conference on Applications of Computer Vision (WACV)*, pages 1109–1117. IEEE, 2019. 2
- [16] Alex Kendall and Yarin Gal. What uncertainties do we need in bayesian deep learning for computer vision? In *Advances in neural information processing systems*, pages 5574–5584, 2017. 2
- [17] Christine Körner and Stefan Wrobel. Multi-class ensemble-based active learning. In *European conference on machine learning*, pages 687–694. Springer, 2006. 2
- [18] David D Lewis and William A Gale. A sequential algorithm for training text classifiers. In *SIGIR’94*, pages 3–12. Springer, 1994. 2
- [19] Buyu Liu and Vittorio Ferrari. Active learning for human pose estimation. In *Proceedings of the IEEE International Conference on Computer Vision*, pages 4363–4372, 2017. 3, 7, 8
- [20] Alexander Ly, Maarten Marsman, Josine Verhagen, Raoul PPP Grasman, and Eric-Jan Wagenmakers. A tutorial on fisher information. *Journal of Mathematical Psychology*, 80:40–55, 2017. 3
- [21] Christoph Mayer and Radu Timofte. Adversarial sampling for active learning. In *Proceedings of the IEEE/CVF Winter Conference on Applications of Computer Vision*, pages 3071–3079, 2020. 2
- [22] Prem Melville and Raymond J Mooney. Diverse ensembles for active learning. In *Proceedings of the twenty-first international conference on Machine learning*, page 74, 2004. 2
- [23] Alejandro Newell, Kaiyu Yang, and Jia Deng. Stacked hourglass networks for human pose estimation. In Bastian Leibe, Jiri Matas, Nicu Sebe, and Max Welling, editors, *Computer Vision – ECCV 2016*, pages 483–499, Cham, 2016. Springer International Publishing. 1, 7
- [24] Dmitry Panchenko. Mit ocv - 18.650:lec31.pdf. http://bit.ly/stats_18-443_lec31, 2003. 4
- [25] Adam Paszke, Sam Gross, Francisco Massa, Adam Lerer, James Bradbury, Gregory Chanan, Trevor Killeen, Zeming Lin, Natalia Gimelshein, Luca Antiga, Alban Desmaison, Andreas Kopf, Edward Yang, Zachary DeVito, Martin Raison, Alykhan Tejani, Sasank Chilamkurthy, Benoit Steiner, Lu Fang, Junjie Bai, and Soumith Chintala. Pytorch: An imperative style, high-performance deep learning library. In H. Wallach, H. Larochelle, A. Beygelzimer, F. d’Alché-Buc, E. Fox, and R. Garnett, editors, *Advances in Neural Information Processing Systems 32*, pages 8024–8035. Curran Associates, Inc., 2019. 7
- [26] Sam T Roweis and Lawrence K Saul. Nonlinear dimensionality reduction by locally linear embedding. *science*, 290(5500):2323–2326, 2000. 4
- [27] Ozan Sener and Silvio Savarese. Active learning for convolutional neural networks: A core-set approach. *arXiv preprint arXiv:1708.00489*, 2017. 2, 3, 7, 8
- [28] Burr Settles. Active learning literature survey. Technical report, University of Wisconsin-Madison Department of Computer Sciences, 2009. 2, 3
- [29] Burr Settles and Mark Craven. An analysis of active learning strategies for sequence labeling tasks. In *Proceedings of*

the 2008 Conference on Empirical Methods in Natural Language Processing, pages 1070–1079, 2008. 3

- [30] Burr Settles, Mark Craven, and Soumya Ray. Multiple-instance active learning. In J. Platt, D. Koller, Y. Singer, and S. Roweis, editors, *Advances in Neural Information Processing Systems*, volume 20. Curran Associates, Inc., 2008. 3
- [31] Shai Shalev-Shwartz and Shai Ben-David. *Understanding machine learning: From theory to algorithms*. Cambridge university press, 2014. 3
- [32] Jamshid Sourati, Murat Akcakaya, Todd K Leen, Deniz Erdogmus, and Jennifer G Dy. Asymptotic analysis of objectives based on fisher information in active learning. *The Journal of Machine Learning Research*, 18(1):1123–1163, 2017. 3
- [33] Ke Sun, Bin Xiao, Dong Liu, and Jingdong Wang. Deep high-resolution representation learning for human pose estimation. In *Proceedings of the IEEE/CVF Conference on Computer Vision and Pattern Recognition (CVPR)*, June 2019. 1
- [34] A. Toshev and C. Szegedy. Deeppose: Human pose estimation via deep neural networks. In *2014 IEEE Conference on Computer Vision and Pattern Recognition*, pages 1653–1660, 2014. 1
- [35] Laurens van der Maaten. Accelerating t-sne using tree-based algorithms. *Journal of Machine Learning Research*, 15(93):3221–3245, 2014. 5
- [36] Laurens Van der Maaten and Geoffrey Hinton. Visualizing data using t-sne. *Journal of machine learning research*, 9(11), 2008. 1, 4, 5
- [37] Yi Yang, Zhigang Ma, Feiping Nie, Xiaojun Chang, and Alexander G Hauptmann. Multi-class active learning by uncertainty sampling with diversity maximization. *International Journal of Computer Vision*, 113(2):113–127, 2015. 2
- [38] D. Yoo and I. S. Kweon. Learning loss for active learning. In *2019 IEEE/CVF Conference on Computer Vision and Pattern Recognition (CVPR)*, pages 93–102, 2019. 2, 3, 7, 8
- [39] Y. Yuan, S. Chung, and H. Kang. Gradient-based active learning query strategy for end-to-end speech recognition. In *ICASSP 2019 - 2019 IEEE International Conference on Acoustics, Speech and Signal Processing (ICASSP)*, pages 2832–2836, 2019. 3
- [40] Ye Zhang, Matthew Lease, and Byron Wallace. Active discriminative text representation learning. In *Proceedings of the AAAI Conference on Artificial Intelligence*, volume 31, 2017. 3

SUPPLEMENTARY MATERIAL

EGL++: Extending Expected Gradient Length to Active Learning for Human Pose Estimation

Megh Shukla

Mercedes-Benz Research and Development India

megh.shukla@daimler.com

Abstract

We briefly discuss the expected gradient length for linear regression formulation presented in the paper. We also draw high-level parallels between the resultant closed form solution and epistemic uncertainty, which we could not due to space constraints in the main paper. Perhaps expected gradient length and bayesian uncertainty are two sides of the same coin?

1. Discussion

We define p, q in the paper as:

$$\begin{aligned} p(x, y|\theta_0) &= p(y|x, \theta_0) p(x) \\ q(x, y) &= \int_{\theta} q(y|x, \theta) q(x) \pi(\theta|z_{obs}) d\theta \end{aligned} \quad (1)$$

Integrating over the posterior distribution $p(\theta|z_{obs})$ is standard practice in Bayesian inference, so why did we invoke the no free lunch theorem? **The No Free Lunch Theorem explains multiple plausible hypothesis which can be quantified using bayesian probability.** We explain this with an example, similar to the one in [6].

Let $\mathcal{X} \in \mathbb{R}^n$ represent a set of values $x_i \in \{-1, 1\}$. Our task is to identify a hypothesis $\theta \in \mathbb{R}^n$ with $\theta_i \in \{-1, 1\}$ such that we maximize $x^T \theta$. This can easily be achieved by initializing $\theta_0 = \mathcal{X}$, with θ_0 representing the only true hypothesis. However, not all values of \mathcal{X} have been observed, adding to the challenge. Let's say we observe the first $m < n$ values of \mathcal{X} , based on which need to select our hypothesis θ . With this new information, we can select any hypothesis where $\theta_{1...m} = x_{1...m}$. Therefore, the number of hypothesis, each equally likely, that explain the first m values is $2^{(n-m)}$.

When $m \ll n$, a large number of plausible hypothesis exist that explain the observations, not just θ_0 [3, 7]. We argue that active learning represents this case, since the

assumption is that we have limited labelled data to begin with. Therefore modelling y with our observed variables is in fact an expectation over all the multiple plausible hypothesis that explain the observed samples z_{obs} .

With the derivation continuing in the main paper, we turn our attention to Eq: (5) from the paper:

$$x^* = \arg \max_{x \in \text{unlabelled}} \left[\frac{1}{K} \sum_{k=1}^K \int_{-\infty}^{\infty} \frac{1}{\sqrt{2\pi} \sigma_k(z_{obs}^{(k)})} \frac{(y - \mu_k(x))^2}{2\sigma_k^2(z_{obs}^{(k)})} [(f_z(x) - y)x]^2 dy \right] \quad (2)$$

Statistical linear regression allows us to model $q(y|x, \theta_k)$ as a normal distribution $\mathcal{N}(\mu_k(x), \sigma_k(z_{obs}))$ [2, 5]. If the objective is $(f_z(x) - y)^2/2$, the gradient for linear regression is: $(f_z(x) - y)x$. In multiple linear regression where there are multiple predictors: $\bar{x} = \{x_1, x_2 \dots x_n\}$ and σ^2 is the unbiased estimate of the mean squared error of the model, the values of μ_k and σ_k for each predictor are:

$$\begin{aligned} \hat{\mu}_k &= \bar{x}^T \theta_k \\ \hat{\sigma}_k &= \sigma_k^2 \bar{x} (X_k^T X_k)^{-1} \bar{x}^T + \sigma_k^2 \end{aligned} \quad (3)$$

We note that both μ and σ are a function of x and differ for each k . We now discuss the closed form solution for expected gradient length - linear regression is:

$$x^* = \arg \max_{x \in \mathcal{U}} \left[\frac{\|x\|^2}{K} \sum_{k=1}^K (\sigma_k^2(x) + (\mu_k(x) - f_z(x))^2) \right] \quad (4)$$

The solution (Eq: 4) has two main components:

1. $\sigma_k^2(x)$: Prediction variance around the mean value \bar{y}
2. $(\mu_k(x) - f_z(x))^2$: The difference between the prediction of the main model f_z and the weak learners θ_k .

Expected gradient length sampling uses two measures of deviation. The first measure corresponds to the prediction variance of a model θ_k for a particular value of input \bar{x} . The second component is straightforward involving the difference in prediction between the main model f_z and the mean prediction of the weak learner θ_k . While the latter term finds interpretation in [1], the closed form solution **Eq: 4** allows us to link expected gradient length for regression to epistemic uncertainty.

1.1. Epistemic Uncertainty in Deep Networks

Kendall and Gal [4] define epistemic uncertainty as:

$$\begin{aligned} \text{Var}(y) &\approx \sigma^2 + \frac{1}{K} \sum_{k=1}^K f_k^2(x) - \left(\frac{1}{K} \sum_{k=1}^K f_k(x) \right)^2 \\ &\approx \frac{1}{K} \sum_{k=1}^K \hat{\sigma}_k^2 + \frac{1}{K} \sum_{k=1}^K f_k^2(x) - \left(\frac{1}{K} \sum_{k=1}^K f_k(x) \right)^2 \end{aligned} \quad (5)$$

We note that $\text{Var}(y)$ corresponds to the epistemic uncertainty, and σ corresponds to the heteroscedastic aleatoric uncertainty for x . The network is trained to predict the output y as well as the aleatoric uncertainty σ for each input x ($f_k : x \rightarrow y, \sigma$), where f_k is the k^{th} dropout model.

1.2. Comparison

A quick glance shows some similarities between **Eq: 4** and **Eq: 5**. We can roughly divide the components in the two equations as the inherent uncertainty in the prediction, and the deviation of the predicted value around the mean. There are subtle differences too. The uncertainty in **Eq: 4** represents the prediction variance whereas the uncertainty in **Eq: 5** represents the learned heteroscedastic aleatoric uncertainty. The other minor differences includes the way in which the deviation around the mean is computed.

Kendall and Gal beautifully apply uncertainties to computer vision using deep learning using dropout as a bayesian approximation. To a much smaller extent, we show that expected gradient length for regression too incorporates model uncertainties in the form of prediction variance. Our solution for linear regression (**Eq: 4**) allows an interpretation of expected gradient length as sampling images with the highest epistemic uncertainty, which we believe to the best of our knowledge that we are the first to do so. So, does generalized expected gradient length converge to sampling with bayesian uncertainties? We hope that a future work answers this question!

References

- [1] W. Cai, Y. Zhang, and J. Zhou. Maximizing expected model change for active learning in regression. In *2013 IEEE 13th International Conference on Data Mining*, pages 51–60, 2013. [2](#)
- [2] Nathaniel Helwig. Multiple linear regression. <http://users.stat.umn.edu/~helwig/notes/mlr-Notes.pdf>, Jan 2017. [1](#)
- [3] Jiaji Huang, Rewon Child, Vinay Rao, Hairong Liu, Sanjeev Satheesh, and Adam Coates. Active learning for speech recognition: the power of gradients, 2016. [1](#)
- [4] Alex Kendall and Yarin Gal. What uncertainties do we need in bayesian deep learning for computer vision? In I. Guyon, U. V. Luxburg, S. Bengio, H. Wallach, R. Fergus, S. Vishwanathan, and R. Garnett, editors, *Advances in Neural Information Processing Systems*, volume 30. Curran Associates, Inc., 2017. [2](#)
- [5] Dmitry Panchenko. Mit ocw - 18.650:lec31.pdf. http://bit.ly/stats_18-443_lec31, 2003. [1](#)
- [6] Shai Shalev-Shwartz and Shai Ben-David. *Understanding machine learning: From theory to algorithms*. Cambridge university press, 2014. [1](#)
- [7] Jamshid Sourati, Murat Akcakaya, Todd K Leen, Deniz Erdogmus, and Jennifer G Dy. Asymptotic analysis of objectives based on fisher information in active learning. *The Journal of Machine Learning Research*, 18(1):1123–1163, 2017. [1](#)